Fusion reactions between ^{32}S and $^{24,25,26}Mg$ in the energy region $E_{lab}=90-150$ MeV

Sl. Cavallaro, Luo Yi Xiao,* and M. L. Sperduto
Dipartimento di Fisica, dell' Universitá di Catania and INFN-Laboratorio Nazionale del Sud, Corso Italia, 57, I-95129 Catania I, Italia
(Received 4 March 1985)

Fusion excitation functions for $^{32}S+^{24,25,26}Mg$ in the incident energy region $E_{lab}=90$ to 150 MeV were measured by means of the in-beam γ-spectroscopy method. In order to suppress background and take into account the contribution of unstable residual nuclei to the in-beam yields of the daughter residues, a computer-controlled chopper system was assembled on the beam line to measure the in-beam and off-beam spectra of the γ rays. Detailed comparison was made between the present measurement and the available data obtained by other methods. The measured A and Z distribution was compared with statistical calculations. The fusion excitation functions, which exhibit a change of slope with respect to low energy data, showing evident limitation on the fusion in this energy region, were analyzed in terms of the interaction barrier model and the statistical yrast line model.

I. INTRODUCTION

It has been experimentally well established[1] that low-energy heavy-ion-induced reactions proceed mainly by the complete fusion mechanism. The fusion cross section, σ_{fus}, when reported as a function of $1/E_{c.m.}$, shows a linear behavior related to the static fusion barrier which can be predicted by the energy density potential calculated by using the sudden approximation.[2]

However, for bombarding energies well above the fusion threshold, serious limitations on the fusion cross section arise which several models try to account for as effects of the entrance channel or compound nucleus system. This energy range, the so-called "region II," is characterized by contributions from the dissipative components of the nuclear interactions and, phenomenologically, by competition between the fusion mechanism and some other strongly damped ones (deep inelastic processes, incomplete fusion, dynamical fission, etc.).[3-5] The energy domains of validity of the two regimes are entrance-channel dependent and neither theoretically nor experimentally well established.

It is therefore interesting to study the detailed behavior of the fusion cross section as a function of the projectile energy, of the charge product Z_1Z_2, and of the mass symmetry of the colliding system. In addition, for light systems, effects of the deformation and isotopic mass of the reacting partners can also be important.

For this purpose we have undertaken the study of the fusion process relative to the reaction $^{32}S+^{24,25,26}Mg$ at some energies well above the Coulomb barrier.

This choice seemed for us very interesting because it involves an intermediate system between $^{20}Ne+^{27}Al$ (Ref. 4) and $^{32}S+^{59}Co$,[5] and for them evidence of some intermediate mechanism between deep-inelastic and fusion processes has been found. In addition, available information about low energy measurements,[6] well reproduced by calculations, could give us a useful reference for the static barrier potential parameters.

In the literature, measurements of the reaction $^{32}S+^{24}Mg$ have already been reported, but some contradiction[7,8] in the high energy region is present. No systematic data for the $^{32}S+^{25}Mg$ and $^{32}S+^{26}Mg$ reactions[8,9] are available. We measured fusion cross sections for the $^{32}S+^{24}Mg$, $^{32}S+^{25}Mg$, $^{32}S+^{26}Mg$ combinations with $E_{lab}=90$ to 150 MeV in steps of 5 MeV to get detailed results in energy regions I and II.

In principle, based on the discrimination between the channels effectively contributing to the fusion from those resulting from different mechanisms, this study needs data coming from the ΔE-E technique, such as A and Z residue identification, angular distributions, and energy spectra. However, in some cases, where there is no ambiguity between the expected mass distribution of the evaporation residues and those coming from other mechanisms, the in-beam γ-spectroscopy method can be used to extract the residue cross sections. This is just the case for our study where the mass distribution of the direct, quasielastic, and deep-inelastic reactions should be centered around the mass $A=32$ of the projectile and $A=24,25,26$ of the targets, while both previous experimental results[9] and realistic statistical calculations indicate that evaporation residues contribute essentially in the mass region of $A \geq 44$.

In view of the facts mentioned above, the in-beam γ-spectroscopy method was chosen, which gives good accuracy provided suitable yrast level schemes of the residual nuclei are available. Mass and charge of the evaporation residues were identified by in-beam measurement of their deexcitation γ rays. Contamination arising from radioactive residues and background has been taken into account by using a computer-controlled chopper system which allows in-beam and off-beam measurements.

The experimental setup and data reduction are described in Sec. II. Experimental results are presented in Sec. III together with the statistical calculations, which

we have done for the mass and charge distribution of the evaporation residues. Section IV is devoted to the analysis of the fusion cross sections. The last section presents a summary and conclusions.

II. EXPERIMENTAL SETUP AND DATA REDUCTION

A. Experimental setup

The experiment was performed at the National Laboratories of Legnaro. The ^{32}S beam, given by the XTU tandem accelerator with energy ranging from 90 to 150 MeV in 5 MeV steps, was suitably focused (a 2×3 mm spot) on the target. In order to get a reasonable counting rate ($\cong$2000 counts/s) and to keep the electronic dead time below a few percent, typical beam currents of 30—80 nA were used, decreasing with the energy of the incident particles.

A Ge(Li) detector and a γ-x HPGe detector with energy resolution at 1332 keV of 2.15 and 1.93 keV, respectively, were put at a distance of $\cong$12 cm from the target at 90 and 55 deg with respect to the beam direction.

In order to take into account the contribution of radioactive decay of unstable residues to the in-beam intensity of the corresponding daughter residual nuclei, in cases where both are produced in the reaction and the lifetimes of the unstable ones are comparable with the measuring time, a computer-controlled chopper system was used. It was assembled on the beam line $\sim$12 m from the well-shielded detectors to allow measurement of γ spectra in in-beam and off-beam conditions. Covered by a thick layer of tantalum, the chopper could be driven to interrupt the beam automatically. The data acquisition and the movement of the chopper system were synchronously controlled by computer. For every run (which consisted typically of 30 s-30 s, 60 complete cycles), four spectra, which were taken at 90 and 55 deg in in-beam and off-beam conditions, respectively, were acquired in turn by the data acquisition system.

This method allows one to directly subtract room background and decay of radioactive nuclei produced in the reaction. The satisfactory solution of radioactive buildup problems enabled us to use the same target for the whole set of a given excitation function measurement.

The target thickness was determined from the energy loss in the target of an alpha beam of $E_{\rm lab}=2$ MeV by measuring the yield of the backing x rays induced by the alpha beam with and without the target.

The target thicknesses were corrected for the isotopic composition of the target. The oxidation and carbon contamination of the target were determined in a separate experiment. The effective thicknesses of ^{16}O and ^{12}C in the target were measured by using the ^{16}O(d,p$_0$)^{17}O, ^{16}O(d,p$_1$)^{17}O*, and ^{12}C(d,p$_0$)^{13}C reactions at $E_{\rm lab}=1.80$ MeV. The proton yields, which were detected by a silicon detector, were normalized to that from a Mylar foil, the thickness (and composition) of which was known. Because of the large cross sections and the simplicity of the spectrum, a good correction of target thicknesses for ^{16}O and ^{12}C was obtained. The overall uncertainty of the thickness values shown in Table I is about 6%.

TABLE I. Composition and thickness of the targets used in the present experiment. Isotopic percentages are from Oak Ridge National Laboratory.

Composition	Target thickness (μg/cm^2) ^{24}Mg	^{25}Mg	^{26}Mg
^{24}Mg	96	9	3
^{25}Mg	a	94	2
^{26}Mg	a	a	173
^{16}O	16	9	77
^{12}C	8	7	16

[a]The effective thickness is negligible.

B. Data reduction

An important point of the present measurement is to assign the measured γ transitions to the corresponding residual nuclei. The assignment was based on the known spectroscopy and performed by using a computer code SEARCH which includes all the level schemes in this mass region.

A residue was considered to be produced in the reaction if all its characteristic yrast transitions were found in the spectra measured at 90 deg after subtraction of the off-beam spectra. For a given residual nucleus, the intensities of all its ground level feedings are a measurement of its production cross section, if the direct particles and high energy γ transitions feeding to the ground state are negligible. From calculations of Ref. 11 it appears that, in this mass and incident energy region, this assumption is correct to 5% of the total ground feeding. The spectra measured at 55°, after subtraction of the off-beam spectra, were used to obtain the intensities of the ground-state feedings of the residual nuclei for every incident energy and for every target-projectile combination. Table II shows the radioactivity properties of the residual nuclei produced in the reactions of interest.

For the determination of the ground-state feeding intensities, special attention was paid to solve the problems of overlapping transitions. In most of the cases the problems were overcome by using known relative intensities and branching ratios from the literature. In a few cases, a comparison between the intensity of the transitions feeding a given level and that deexciting it was made to give a limit on the intensity of the unresolved transition.

For the correction for contamination of ^{16}O and ^{12}C in the 44,45,46 mass region, the contamination was estimated by taking into account the intensities of the ground-feeding γ transitions obtained for the ^{32}S+^{16}O and ^{32}S+^{12}C reactions from some low, middle, and high energy measurements we made, and by interpolating for the remaining energies. It is worth noting that the "add back" procedure with a chopper system is necessary to determine the correct ground-state feeding intensity for a residual nucleus which deexcites via an isomer state. The intensity measured in the off-beam spectrum should be added back to that measured in the in-beam spectrum to give the true intensity. The 3041 keV ($\frac{19}{2}^-$) isomer state of ^{53}Fe, for instance, deexcites uniquely to the 2339 keV ($\frac{11}{2}^-$) level via an $E4$ transition with a lifetime of 2.53

TABLE II. Radioactivity from $^{32}S+^{24,25,26}Mg$ reactions in the 90–150 MeV laboratory incident energy range. An asterisk indicates the excited level.

Reaction	Nucleus	Decay	$T_{1/2}$	Daughter	$T_{1/2}$	E_γ (keV)
$^{32}S+^{24}Mg$	^{48}V	β^+ EC	15.9 d	$^{48}Ti^*$	stable	1312,983
	^{48}Cr	EC	21.56 h	$^{48}V^*$	stable	116,308
	^{51}Mn	β^+ EC	46.2 min	$^{51}Cr^*$	27.7 d	749
	^{52}Mn	β^+ EC	5.59 d	$^{52}Cr^*$	stable	744,936,1434
	$^{52}Mn(2^+)$	EC	21.1 min	$^{52}Cr^*$	stable	1434
	^{53}Fe	β^+	8.51 min	$^{53}Mn^*$	stable	377
$^{32}S+^{25}Mg$	^{48}V	β^+ EC	15.9 d	$^{48}Ti^*$	stable	1312,973
	^{48}Cr	EC	21.56 h	$^{48}V^*$	stable	116,308
	^{51}Mn	β^+ EC	46.2 min	$^{51}Cr^*$	27.7 d	749
	^{52}Mn	β^+ EC	5.59 d	$^{52}Cr^*$	stable	744,936,1434
	$^{52}Mn(2^+)$	β^+ EC	21.1 min	$^{52}Cr^*$	stable	1434
	^{53}Fe	β^+	8.51 min	$^{53}Mn^*$	stable	377
$^{32}S+^{26}Mg$	^{48}V	β^+ EC	15.9 d	$^{48}Ti^*$	stable	1313,983
	^{51}Cr	EC	27.7 d	$^{51}V^*$	stable	320
	^{51}Mn	β^+ EC	46.2 min	$^{51}Cr^*$	27.7 d	749
	^{52}Mn	β^+ EC	5.59 min	$^{52}Cr^*$	stable	744.936,1434
	$^{52}Mn(2^+)$	β^+ EC	21.1 min	$^{52}Cr^*$	stable	1434
	^{53}Fe	β^+	8.51 min	$^{53}Mn^*$	stable	377

min. Its ground-state feeding was found almost to disappear in the spectra with subtraction of off-beam spectra because the in-beam and off-beam spectra share its intensity.

The ground-state feeding intensities were then used to obtain the absolute cross section by normalizing them to the Coulomb excitation cross section of the 547 keV transition of the Au backing, which was calculated following the formalism of Ref. 10, regarding the backing as a target of infinite thickness.

The partial cross section for a given residual nucleus formed in a fusion-evaporation reaction is thus given by

$$\sigma_i(E)=\sigma_{CE}(E)\frac{A_{Mg}B_{547}}{A_{Au}D_{Mg}}\frac{\Sigma I_k/\varepsilon_k}{I_{547}/\varepsilon_{547}} \quad (1)$$

in which E is the incident energy; A_{Mg} and A_{Au} represent the mass number of the target and backing, respectively; D_{Mg} is the target thickness, B_{547} and I_{547} are the branching ratio and the intensity of the 547 keV γ ray of Au; I_k is the intensity of the ground-state feeding kth transition; ε_k and ε_{547} express their relative detection efficiency, respectively; and $\sigma_{CE}(E)$ is the thick-target integral for Coulomb excitation of the $E^*=547$ keV, $J=\frac{7}{2}^+$ state in ^{197}Au.

Contamination from isotopic composition was taken into account. For the $^{32}S+^{x}Mg$ combination, the correction of partial cross sections for isotropic contamination from $^{32}S+^{y}Mg$ was made according to the equation

$$\sigma_i^x(E)=\sigma_i^{x'}(E)-\sigma_i^y(E)\frac{D^{\text{eff}}_{^yMg}}{D^{\text{eff}}_{^xMg}}, \quad (2)$$

where $\sigma_i^{x'}(E)$ is the partial cross section determined by using the effective thickness of ^{x}Mg in the target and the ground-state feeding intensities experimentally measured (which include the contribution of $^{32}S+^{y}Mg$), $\sigma_i^y(E)$ is the cross section of the same residual nucleus from the $^{32}S+^{y}Mg$ combination, and $D^{\text{eff}}_{^xMg}$ and $D^{\text{eff}}_{^yMg}$ represent the effective thickness of ^{x}Mg and ^{y}Mg in the ^{x}Mg target. For the $^{32}S+^{25}Mg$ and $^{32}S+^{26}Mg$ combinations, the partial and total fusion cross sections were corrected according to the above-described method.

Statistical errors on experimental peak areas were usually negligible. Taking into account the systematic errors due to target thickness, Coulomb excitation yields, relative efficiency calibrations, and contamination corrections, the total errors on absolute partial cross sections have been estimated to be between 10% and 15%, depending on the bombarding energy.

III. EXPERIMENTAL RESULTS

A. Residue cross sections

A complete list of the observed residual nuclei and the energies of the γ-ray transitions used for determining their production cross section are reported in Table III.

In Figs. 1–3 samples of evaporation residue cross sections are reported to show their main features and to compare our results with the existing data in the literature and with statistical calculations. Figure 1 reports our data on the cross sections for each Z and A evaporation residue at $E_{lab}=130$ MeV for $^{32}S+^{24}Mg$, $^{32}S+^{25}Mg$, and $^{32}S+^{26}Mg$, as well as the results of the code CASCADE,[12] for the same reactions and energy.

In order to compare the experimental results with those obtained from the ΔE-E technique, the mass distribution for $E_{lab}=130$ MeV (our work) is shown in Fig. 2 together with that presented in Ref. 9. The comparison exhibits on average a good agreement of our results with literature values and statistical predictions, showing the validity of the in-beam γ spectroscopy method.

TABLE III. List of the observed residual nuclei and energies of the γ transitions used in the determination of the residue cross sections.

Nucleus	E_γ (keV)	Nucleus	E_γ (keV)	Nucleus	E_γ (keV)	Nucleus	E_γ (keV)
^{44}Sc	350	^{48}V	428	^{50}Cr	738	^{54}Mn	156
^{44}Sc	1237		613	^{51}Cr	1165		368
	1662		627		1480		839
^{45}Ti	1469	^{49}V	1021		749		408
^{46}Si	889	^{50}V	910		1353	^{53}Fe	1328
^{47}Ti	159		226	^{52}Cr	1434		2339
^{48}Ti	984		1725	^{51}Mn	238	^{54}Fe	742
^{46}V	915	^{51}V	1609		1139		1407
	801		1813	^{52}Mn	870	^{55}Fe	1317
^{47}V	146	^{48}Cr	752		2286		931
^{48}V	308	^{49}Cr	271	^{53}Mn	1441		1409

Figure 3 presents some of the excitation functions relative to the same outgoing channels, as well as statistical calculations using the CASCADE code of Puhlhofer.[12] These calculations have been done using the parameters suggested by the author, and the known yrast level schemes of the $A=40$–60 mass region. The transmission coefficients of the entrance channel have been computed by assuming a diffuseness of 1 fm. To take into account the small deformation effects in this mass region, the following values have been used for the strengths of the electromagnetic transitions: $E1=5\times10^{-4}$; $M1=2.8\times10^{-2}$; $E2=1.4$ W.u. Table V reports the parameter values adopted in the CASCADE calculations.

From an inspection of Fig. 3, it appears that the α2pn and α3p channels present the same trend, independent of the combination we consider, and that the agreement with the statistical calculations is satisfactory, showing the evaporative nature of the processes. The α2p channel is reproduced with regard to energy dependence, but the absolute yield is not in agreement with CASCADE results. A detailed study of the excitation function of the residues will be given in a forthcoming paper.[20]

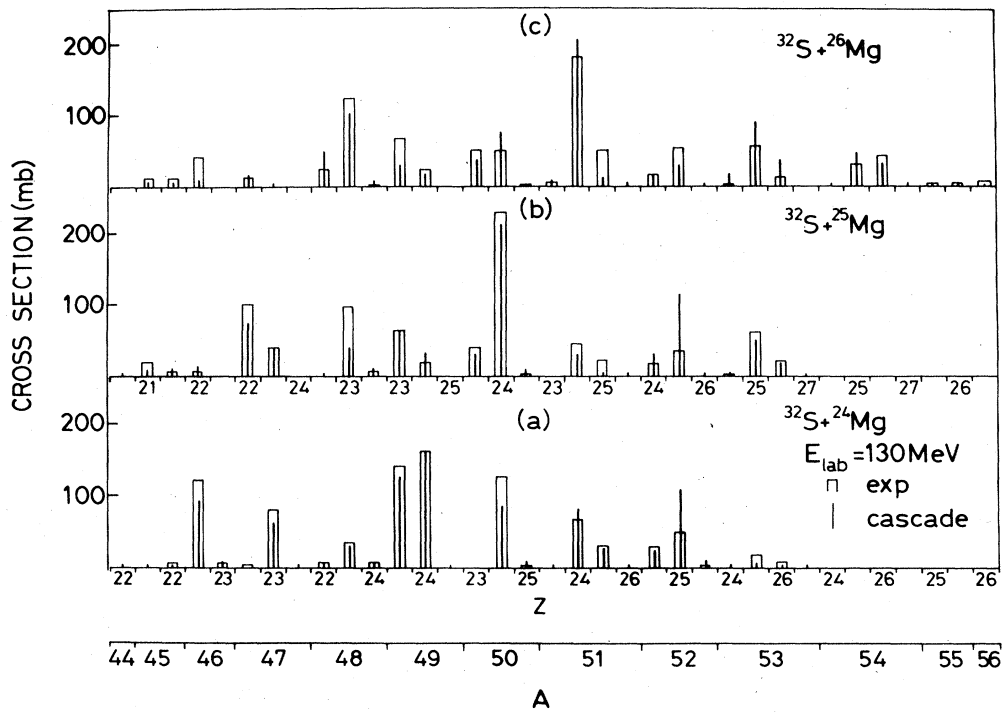

FIG. 1. Measured residue charge and mass distribution and statistical-model calculations at $E_{lab}=130$ MeV. (a) for the ^{32}S+^{24}Mg reaction; (b) for the ^{32}S+^{25}Mg reaction; (c) for the ^{32}S+^{26}Mg reaction.

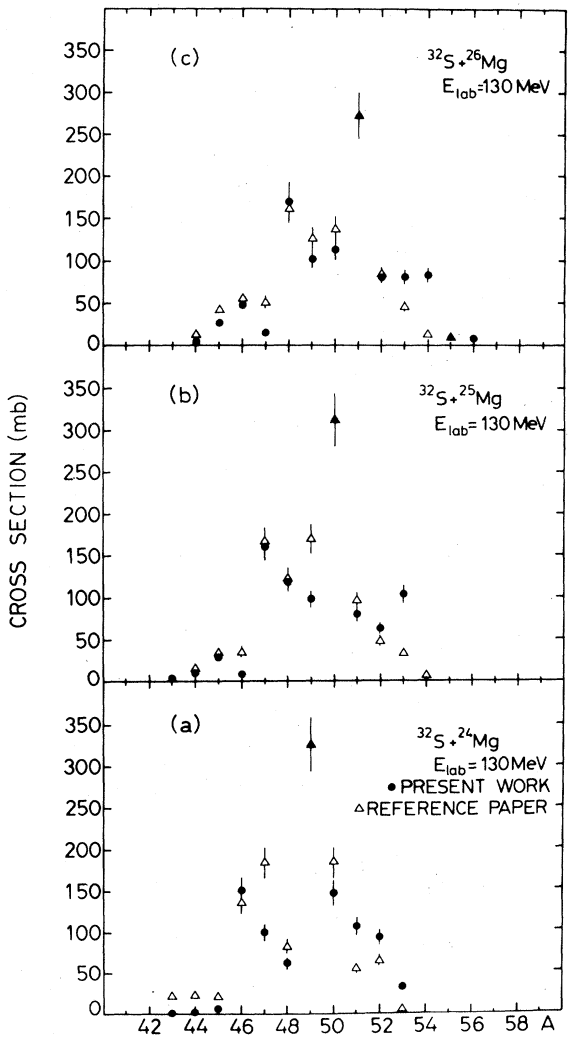

FIG. 2. Comparison of the measured mass distribution at $E_{lab}=130$ MeV with the same data from the ΔE-E technique (Ref. 9) (a) for the $^{32}S+^{24}Mg$ reaction; (b) for the $^{32}S+^{25}Mg$ reaction; (c) for the $^{32}S+^{26}Mg$ reaction.

B. Fusion cross sections

By summation of all the experimental partial cross sections, the total fusion cross section values have been obtained for all three systems in the energy range as specified in Table IV. These results are presented in Fig. 4, together with the low-energy results of Ref. 6. In comparison with these last results our data show a large change in the slope characteristic of strong limitations on the fusion mechanism, and large contributions to the reaction cross section from other mechanisms. This is also shown quantitatively in Fig. 5, where the grazing angular momentum and the critical angular momentum as a function of $E_{c.m.}$ are reported.

For the $^{32}S+^{24}Mg$ fusion excitation function, our results are in agreement with those of Ref. 23 within the experimental errors, although their general trend seems to be lower. A high energy extrapolation of our results is consistent with data of Ref. 8, at $E_{lab}=160$ MeV, indicating a decrease of cross section with increasing energy.

IV. ANALYSIS OF FUSION CROSS SECTIONS

Fusion between a bombarding nucleus (Z_1,A_1) and a target nucleus (Z_2,A_2), with relative kinetic energy $E_{c.m.}$, occurs when the intermediate system formed lives for a time long enough to allow its angular momentum and excitation energy to be shared between the individual nucleons of the system. Under these conditions thermalization is obtained and emission of light particles such as n, p, α, and γ presents the characteristic of compound nucleus evaporation.

The simplest way to understand the mechanism leading to the fusion process is given by the interaction barrier model. For energies $E_{c.m.}$ just above the Coulomb barrier fusion will occur for all partial waves which satisfy the condition

$$V_l(R_l)\leq E_{c.m.}\ , \tag{3}$$

i.e., if the height of the barrier experienced by a particular l wave $V_l(R_l)$ at its maximum position R_l is lower than $E_{c.m.}$.

In this picture it is assumed that strong friction forces will be able to reduce the kinetic energy of all l components which overcome the height of the barrier, so that fusion will occur, provided only that a pocket in the potential is present. This model introduces the concept of the critical angular momentum and predicts the linear behavior of σ_{fus} as a function of $1/E_{c.m.}$.

Disappearance of the pocket in the total potential curve gives rise to larger limitations on the fusion mechanism. In fact, it is necessary that each l wave contributing to fusion reach a critical distance R_{cr} in order to allow friction forces to reduce the kinetic energy and to bring the system to fuse.

TABLE IV. The energy intervals and fusion excitation functions measured in the present work.

Target-projectile combination	CN	Coulomb barrier (MeV)	Incident energy (MeV)[a] Laboratory	c.m.	Excitation energy of CN (MeV)
$^{32}S+^{24}Mg$	^{56}Ni	31.7	89.1—149.3	38.2—64.0	52.2—78.0
$^{32}S+^{25}Mg$	^{57}Ni	31.5	89.1—149.3	39.1—65.5	56.0—82.4
$^{32}S+^{26}Mg$	^{58}Ni	31.3	87.8—148.2	39.4—66.4	57.4—84.4

[a]The incident energies have been corrected for energy losses in the target.

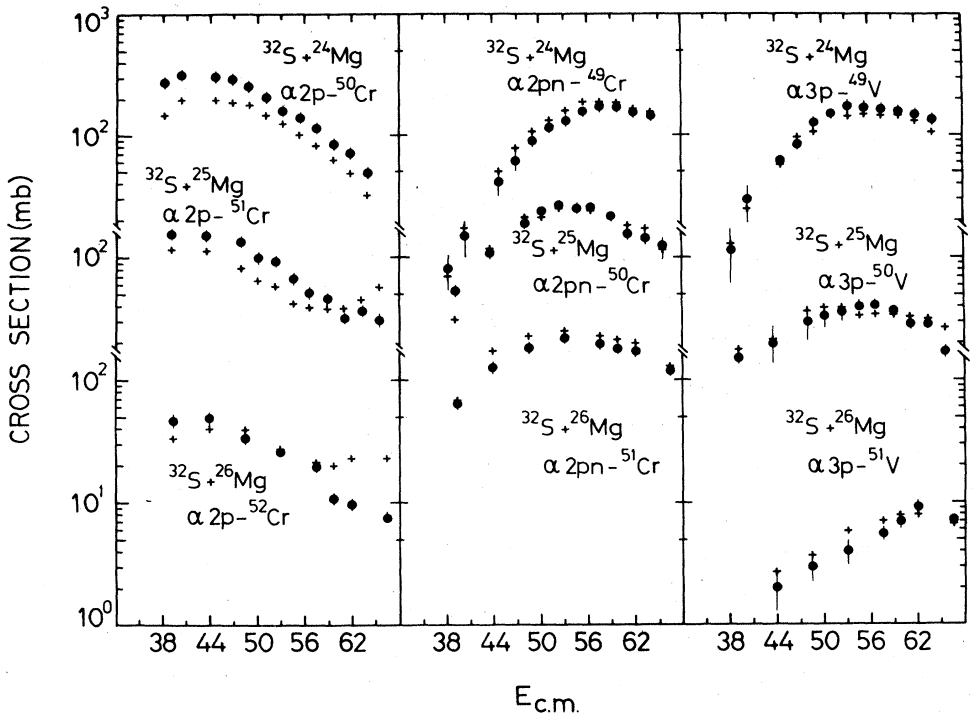

FIG. 3. Experimental excitation functions for the α2p, α3p, and α2pn outgoing channels. The crosses correspond to the statistical-model calculations done by means of the CASCADE code (Ref. 12).

TABLE V. Parameters for the CASCADE statistical calculations. Nomenclature as in Ref. 12.

Angular momentum distribution in the compound nucleus
Maximum angular momentum L derived from σ_{fus}; diffuseness $d=1$ fm
Optical potentials for emitted particles:
Neutrons, Wilmore and Hodgson (Ref. 13)
Protons, Perey (Ref. 14)
α particles, Huizenga and Igo (Ref. 15)
Decay strengths
$(E1)=0.0005$ W.u.
$(M1)=0.028$ W.u. [Bertrand, Martinot, and Verges (Ref. 16)]
$(E2)=1.4$ W.u.
Level density parameters
Region I ($E^* \leq 4$ MeV)
Discrete levels as far as known experimentally (Ref. 17 and references therein)
Region II (4 MeV $\leq E^* \leq 7.5$ MeV)
Fermi gas level density formula (Ref. 18) with empirical a and Δ from Dilg *et al.* (Ref. 19)
Effective moment of inertia $\mathcal{I}=0.85\mathcal{I}_{rigid}$ (or $r_0=1.18$ fm)
Known-spin states included as yrast levels
Region III ($E \geq 15$ MeV)[a]
Fermi gas level density parameters $a_{LDM}=A/8.$ MeV^{-1}
Moment of inertia for rigid body
Radius parameter $r_0=1.28$ fm
Deformation from liquid-drop theory
Deformability $\delta=10^{-4}$[b]

[a]The level density parameters are linearly interpolated between regions II and III.
[b]Used to calculate the effective moment of inertia $\mathcal{I}=\mathcal{I}_{sphere}(1+\delta L^2)$.

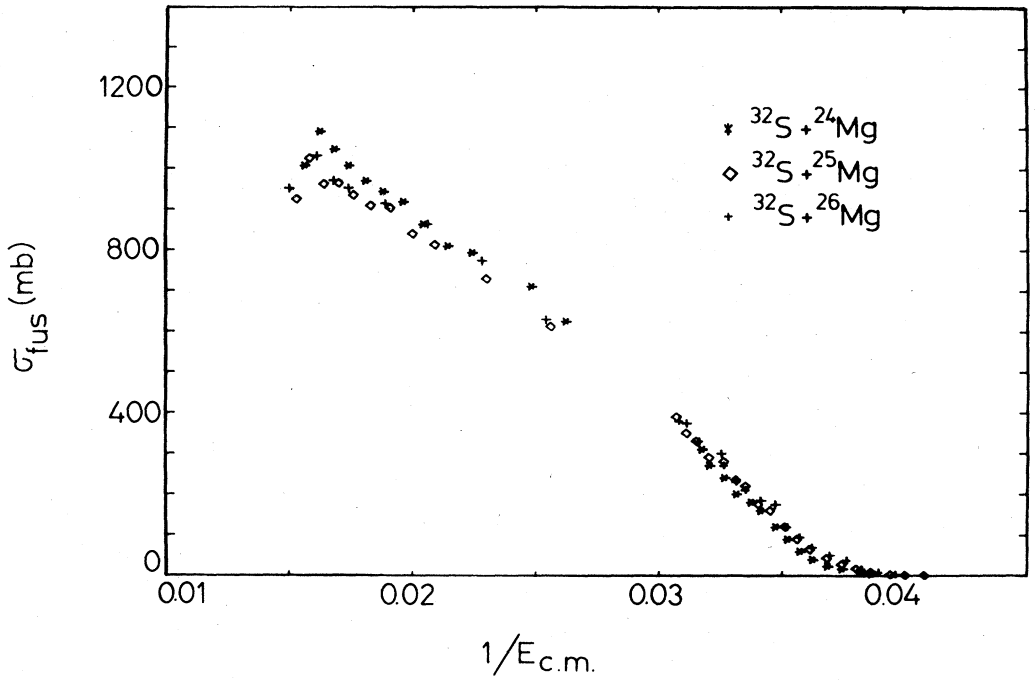

FIG. 4. Experimental fusion cross section vs $1/E_{c.m.}$ for the $^{32}S+^{24}Mg$, $^{32}S+^{25}Mg$, and $^{32}S+^{26}Mg$ reactions. Low energy data are from Ref. 6.

The main problem of this model is how to determine the nuclear part of the potential. In the sudden approximation it is assumed that the density of the two nuclei remains frozen during the collision. The relative motion between the two nuclei is fast enough for the densities not to change. This approximation fits very well data at low energy where the fusion process is determined during the earlier stages of the interaction (the interaction barrier regime).

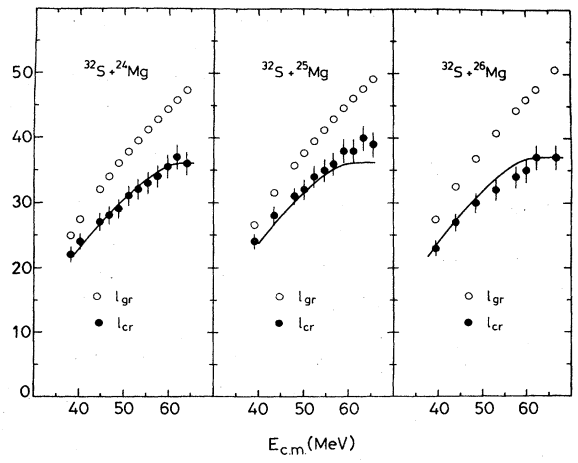

FIG. 5. Grazing and critical angular momenta versus the center of mass energy. l_{gr}=grazing angular momentum, l_{cr}=critical angular momentum, both in $\hbar$ units. l_{cr} has been calculated by the equation $\sigma_{fus}=\pi\lambda\!\!\!^{-2}(l_{cr}+1)^2$.

The adiabatic approximation works in the opposite direction and assumes that the relative motion is slow enough for the system to have time to share energy between other degrees of freedom (such as surface vibrations or neck formation), and to reach a relaxed configuration. Calculations based on this approximation are able to explain the fission saddle configuration and seem to indicate that the static potential barrier model is too simple to explain fusion at high energies as those concerned in the critical distance regime (regime II).

Our data domain is actually lying in the first regime and only for the last point at $E_{lab}=150$ MeV does it seem that regime II is reached. However, comparison with data of Ref. 6 shows a change of slope which is unexpected in a rough analysis of the interaction barrier regime conditions. In effect the well-known linear equation

$$\sigma_{fus}=\pi R_0^2\left[1-\frac{V(Q_0)}{E_{c.m.}}\right] \tag{4}$$

is obtained in the approximation that the position of the fusion barrier for a given l, R_l, does not depend too much on l, i.e., $R_l \simeq R_0$ for

$$l < l_{cr} \ . \tag{5}$$

This is a good approximation only if l_{cr} is not too large, where l_{cr} is the value of l for which $V_{l_{cr}}(R_{l_{cr}})=E_{c.m.}$, and

$V_{l_{cr}}(R_{l_{cr}})$ is the height of the total barrier including the centrifugal term

$$l_{cr}(l_{cr}+1)\hbar^2/2\mu R_{l_{cr}}^2 \ . \quad (6)$$

For energies well above the Coulomb barrier as in our experimental conditions, approximation (5) is really not good enough, so that Eq. (4) is not valid. We may then ascribe to this fact the change of the slope with respect to the data at low energy in Fig. 4.

To show this effect quantitatively, we calculated the height and the position of the interaction barrier for each $E_{c.m.}$ value of our experimental domain and for the corresponding l_{cr}.

Following the parametrization of Ngô[24] for the nuclear part of the potential, we assumed

$$V_n(R)=C_1C_2/(C_1+C_2)U_n(s)$$

with $s=R-C_1-C_2$, where the C_i's are the central radii of isolated nuclei, defined by

$$C_i=R_i(1-1/R_i^2) \ ,$$

where $R_i=1.16A^{1/3}$ and

$$U_n(s)=-34\exp-[(s+1.6)^2/5.4]$$

for $s>-1.6$ fm and

$$U_n(s)=-34+5.4(s+1.6)^2$$

for $s<-1.6$ fm.

The Coulomb interaction potential has been calculated by assuming spherical nuclei of charge Z_1 and Z_2 and following the parametrization of Ref. 25.

Figure 6 reports $R_{l_{cr}}$ as a function of $E_{c.m.}$ for each value of $E_{c.m.}$ which satisfies Eq. (3). From this figure we can see that the position of the maximum of the barrier, $R_{l_{cr}}$, is very different from that which is assumed for $l=0$ from low energy data ($R_0\cong 9.20$ fm), and it decreases until it reaches the value of 5.6 fm corresponding to conditions where the potential loses the attractive char-

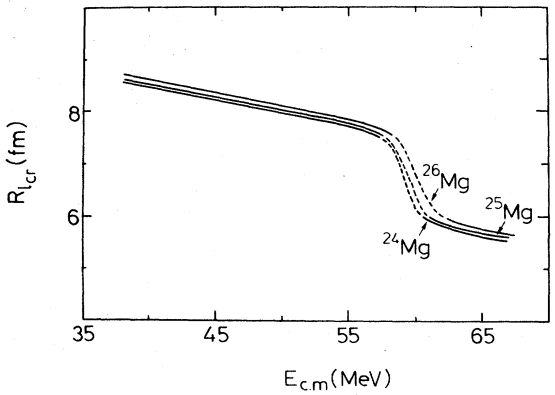

FIG. 6. Radius of the barrier at its maximum, for each critical angular momentum, vs $E_{c.m.}$.

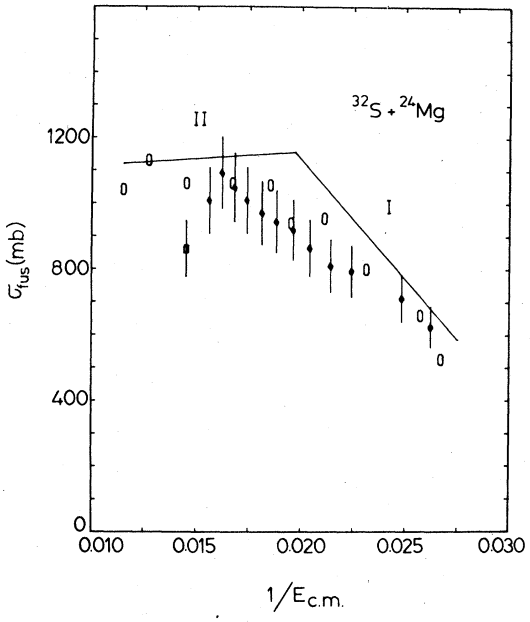

FIG. 7. Experimental fusion excitation function of the ^{32}S+^{24}Mg reaction together with some model predictions. Experimental values are reported with their absolute errors as a function of $1/E_{c.m.}$. The open circle and open square indicate the results of Ref. 23 and Ref. 8, respectively. The solid line represents the results of the "statistical yrast line" model of Ref. 22, obtained by using the following parameters; $R=9.10$ fm, $V=20.18$ MeV (values taken from the low-energy data of Ref. 6), and $\Delta Q=10$ MeV.

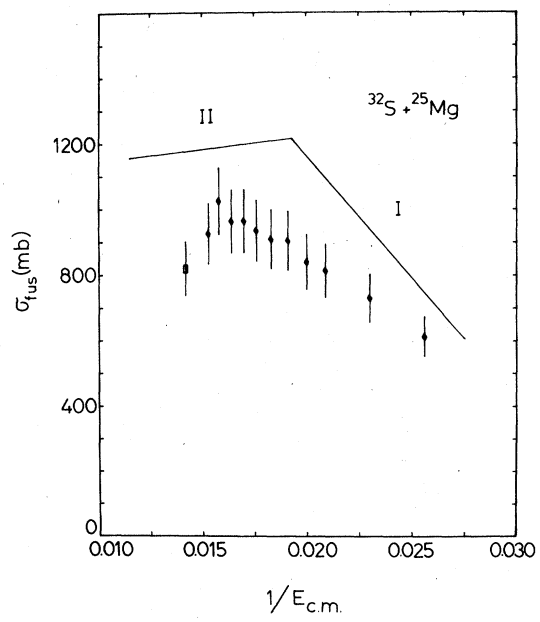

FIG. 8. The same as Fig. 7 for the ^{32}S+^{25}Mg reaction. $R=9.17$ fm, $V=27.99$ MeV (values taken from the low-energy data of Ref. 6), and $\Delta Q=10$ MeV. The open square indicates the results of Ref. 8.

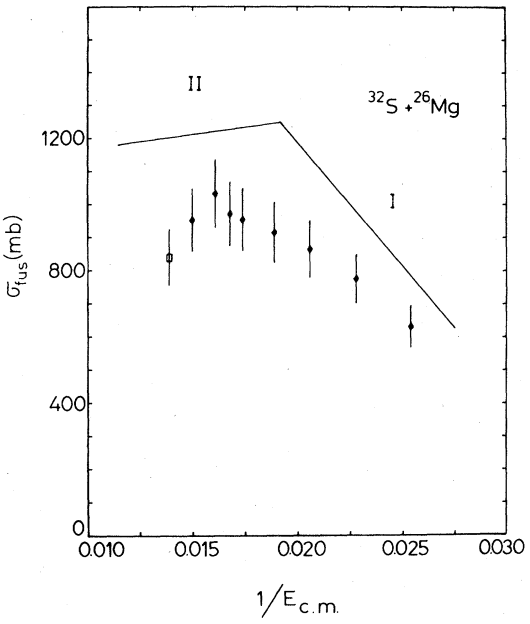

FIG. 9. The same as Fig. 6 for the $^{32}S+^{26}Mg$ reaction. $R=9.24$ fm, $V=27.80$ MeV (values taken from the low-energy data of Ref. 6), and $\Delta Q=10$ MeV. The open square indicates the results of Ref. 8.

acter of the pocket (regime II, or the critical distance regime).

It is interesting to observe that this nuclear potential parametrization is able to explain our expermental data, as shown by the agreement between our experimental critical angular momentum l_{cr} values and those of continuous curve of Fig. 5 [Eq. (3)]. It is also worth observing that high energy saturation of the cross section is predicted by the above-mentioned parametrization.

Predictions of the "statistical yrast line" model of Arima *et al.*[21,22] for regime II are reported in Figs. 7–9. They have been obtained by using values taken from low energy data for the interaction barrier parameters (regime I) and indicate that this model rather overestimates the experimental fusion cross sections.

V. SUMMARY AND CONCLUSIONS

In this paper we have presented the results characterizing the fusion-evaporation process between the ^{32}S nucleus and the $^{24,25,26}Mg$ isotopes, for energies ranging from values well above the Coulomb barrier to those where the saturation of the cross section begins. The main feature of these reactions is the evident limitation of the fusion process as is shown by the change in slope of the cross section behavior and by the values of the critical angular momentum we found.

At this energy, within the experimental errors, there is no evidence that the fusion process depends on the isotopic mass of the colliding system.

For $E_{lab} < 150$ MeV the static interaction barrier model with an l-dependent position of the maximum of the barrier $R_{l_{cr}}(l)$ can account for the experimental fusion cross sections.

For $E_{lab} \geq 150$ MeV it seems that regime II is reached and that the critical distance, which corresponds to the disappearance of the pocket potential, is governing the fusion mechanism. However, in this last regime better descriptions should be obtained by dynamical trajectory models, such as that of Birkelund *et al.*,[23] where contributions of radial and tangential friction are explicitly included, or by the dynamical fusion model of Ngô,[24] where effects of dynamics on the shape of the nuclear potential are taken into account.

ACKNOWLEDGMENTS

The authors wish to thank Prof. M. Morando for his kind cooperation in preparing software to control the chopper system, as well as Dr. F. Giustolisi and Mr. D. Nicotra for hardware design and assembly. They want also to express their thanks to Prof. R. A. Ricci and C. Signorini for their kind hospitality at the National Laboratories of Legnaro of the INFN.

*On leave from Institute of Modern Physics, Academia, Sinica, Lanzhou, China.

[1]L. C. Vaz, J. M. Alexander, and R. G. Satchler, Phys. Rep. **69**, 373 (1981); H. J. Krappe, Vol 117 of *Lecture Notes in Physics*, edited by W. von Oertzen (Springer, New York, 1980), p. 312; D. M. De Castro Rizzo, E. Bozek, S. Cavallaro, B. Delaunay, J. Delaunay, H. Dumont, M. G. Saint Laurent, and F. Terrasi, Nucl. Phys. **A427**, 151 (1984).

[2]D. Dalili, R. Lucas, C. Ngô, T. Suomijarvi, and E. Tomasi, in Proceedings of the International Conference on the Theoretical Approach to the Heavy Ion Reaction Mechanism, Commissariat à l'Energie Atomique Report CEA-N-2406, 1984, p. 91.

[3]W. U. Schroder, P. J. R. Birkelund, J. R. Huizenga, K. L. Wolf, J. P. Unik, and V. E. Viola, Phys. Rev. Lett. **36**, 514 (1976); J. Barrette, P. Braun-Munzinger, C. K. Gelbke, E. Grosse, H. J. Harney, J. Kuzminski, I. Tserruya, and Th. Walcher, Z. Phys. A **274**, 121 (1975); R. Vandenbosch, M. P. Webb, and T. D. Thomas, Phys. Rev. Lett. **36**, 459 (1976); J. B. Natowitz, M. N. Namboodiri, and E. T. Chulick, Phys. Rev. C **13**, 171 (1976).

[4]J. B. Natowitz, M. N. Namboodiri, R. Eggers, P. Gonthier, K. Geoffroy, R. Hanus, C. Towsley, and K. Das, Nucl. Phys. **A277**, 477 (1977).

[5]I. Iori, M. Gentili, I. Massa, G. Vannini, P. Boccaccio, G. Reffo, L. Vannucci, and R. A. Ricci, Phys. Lett. **132B**, 304 (1983); J. P. Coffin, C. Guillaume, A. Fahli, F. Rami, B. Heusch, P. Wagner, P. Engelstein, P. Fintz, and N. Cindro, Phys. Rev. C **30**, 539 (1984).

[6]G. M. Berkowitz, P. Braun-Munzinger, J. P. Karp, R. H.

Freifelder, T. R. Renner, and H. W. Wilschut, Phys.Rev. C **28**, 667 (1983).

[7]H. H. Gutbrod, N. G. Winn, and M. Blann, Nucl. Phys. **A213**, 267 (1973); D. G. Kovar, P. D. Bond, C. Flaum, M. J. Levine, and C. E. Thorn, Bull. Am. Phys. Soc. **22**, 66 (1977).

[8]F. Puhlhofer, W. F. W. Schneider, F. Busch, J. Barrette, P. Braun-Munzinger, C. K. Gelbke, and H. E. Wegner, Phys. Rev. C **16**, 1010 (1977).

[9]T. M. Cormier, E. R. Cosman, A. J. Lazzarini, H. E. Wegner, J. D. Garrett, and F. Puhlhofer, Phys. Rv. C **15**, 654 (1977).

[10]K. Alder, A. Bohr, T. Hnus, B. Mottelson, and A. Winther, Rev. Mod. Phys. **28**, 432 (1956).

[11]S. Cavallaro and J. Delaunay, Commissariat à l'Energie Atomique Report CEA-N-2385, 1984, p. 33; S. Cavallaro *et al.* (unpublished).

[12]F. Puhlhofer, Nucl. Phys. **A280**, 267 (1977).

[13]D. Wilmore and P. E. Hodgson, Nucl. Phys. **55**, 673 (1964); P. E. Hodgson, Annu. Rev. Nucl. Sci. **17**, 1 (1967).

[14]F. G. Perey, Phys. Rev. **131**, 745 (1963).

[15]J. R. Huizenga and G. Igo, Nucl. Phys. **29**, 462 (1961).

[16]F. Bertrand, M. Martinot, and N. Verges, in IAEA Report IAEA-SM-170/60, 1973, Vol. II.

[17]A. D'Onofrio, H. Dumont, M. G. Saint Laurent, B. Delaunay, F. Terrasi, and J. Delaunay, Nucl. Phys. **A378**, 111 (1982).

[18]D. W. Lang, Nucl. Phys. **77**, 545 (1966).

[19]W. Dilg, W. Schantl, H. Vonach, and M. Uhl, Nucl. Phys. **A217**, 269 (1973).

[20]S. Cavallaro, Luo Yi Xiao, and M. L. Sperduto (unpublished).

[21]S. M. Lee, T. Matsuse, and A. Arima, Phys. Rev. Lett. **45**, 165 (1980).

[22]T. Matsuse, A. Arima, and S. M. Lee, Phys. Rev. C **26**, 2338 (1982).

[23]J. R. Birkelund, L. E. Tubbs, J. R. Huizenga, J. N. De, and D. Sperber, Phys. Rep. **56**, 107 (1979).

[24]C. Ngô, in Proceedings of the International Conference on Nuclear Physics, Florence, 1983, edited by P. Blasi and R. A. Ricci, Vol. II, p. 321.

[25]J. Wilczynski and K. Siwek-Wilczynska, Phys. Lett. **55B**, 270 (1975).